Stem Cell Reports
Article

ISSCR

OPEN ACCESS

Characterization of hiPSC-Derived Muscle Progenitors Reveals Distinctive Markers for Myogenic Cell Purification Toward Cell Therapy

Minas Nalbandian,[1] Mingming Zhao,[1,*] Mitsuru Sasaki-Honda,[1] Tatsuya Jonouchi,[1] Antonio Lucena-Cacace,[2] Takuma Mizusawa,[3] Masahiko Yasuda,[3] Yoshinori Yoshida,[2] Akitsu Hotta,[1] and Hidetoshi Sakurai[1,*]

[1]Department of Clinical Application, Center for iPS Cell Research and Application (CiRA), Kyoto University, 53 Shogoin-Kawahara-cho, Sakyo-ku, Kyoto 606-8507, Japan

[2]Department of Cell Growth and Differentiation, Center for iPS Cell Research and Application (CiRA), Kyoto University, 53 Shogoin-Kawahara-cho, Sakyo-ku, Kyoto 606-8507, Japan

[3]Central Institute for Experimental Animals, 3-25-12 Tonomachi, Kawasaki-ku, Kawasaki 210-0821, Japan

*Correspondence: zhaoming@cira.kyoto-u.ac.jp (M.Z.), hsakurai@cira.kyoto-u.ac.jp (H.S.)

https://doi.org/10.1016/j.stemcr.2021.03.004

SUMMARY

The transplantation of muscle progenitor cells (MuPCs) differentiated from human induced pluripotent stem cells (hiPSCs) is a promising approach for treating skeletal muscle diseases such as Duchenne muscular dystrophy (DMD). However, proper purification of the MuPCs before transplantation is essential for clinical application. Here, by using *MYF5* hiPSC reporter lines, we identified two markers for myogenic cell purification: CDH13, which purified most of the myogenic cells, and FGFR4, which purified a subset of MuPCs. Cells purified with each of the markers showed high efficiency for regeneration after transplantation and contributed to the restoration of dystrophin expression in DMD-immunodeficient model mice. Moreover, we found that MYF5 regulates *CDH13* expression by binding to the promoter regions. These findings suggest that FGFR4 and CDH13 are strong candidates for the purification of hiPSC-derived MuPCs for therapeutical application.

INTRODUCTION

During skeletal muscle regeneration, a local resident stem cell population called satellite cells (SCs) (Mauro, 1961) plays a fundamental role in the maintenance and repair of the tissue (Relaix and Zammit, 2012). The transplantation of healthy SCs has been studied as regenerative medicine for skeletal muscle disease (Cerletti et al., 2008; Marg et al., 2014; Montarras et al., 2005; Sacco et al., 2008; Tanaka et al., 2009; Xu et al., 2015). However, isolating human SCs from a human biopsy is challenging and invasive. In addition, *in vitro* expansion of SCs causes the loss of their regeneration potential, resulting in senescence (Gilbert et al., 2010; Montarras et al., 2005; Negroni et al., 2009). On the other hand, human induced pluripotent stem cells (hiPSCs) can be expanded and then differentiated to various cell lineages (Takahashi et al., 2007), making them an attractive cell source for generating muscle progenitor cells (MuPCs).

Indeed, several groups (Chal et al., 2015; Darabi et al., 2012; Sato et al., 2019; Shelton et al., 2014; Wu et al., 2018; Xi et al., 2017; Zhao et al., 2020) have developed *in vitro* differentiation systems to obtain MuPCs from hiPSCs (hiPSC-MuPCs). However, many of these methods artificially overexpress myogenic factors to induce the skeletal muscle differentiation (Darabi et al., 2012; Sato et al., 2019), which currently limits their clinical use because of potential tumorigenicity due to random integration. To avoid this risk, transgene-free differentiation protocols have also been developed (Chal et al., 2015; Shelton et al., 2014; Wu et al., 2018; Xi et al., 2017; Zhao et al., 2020).

Although hiPSC-MuPCs show myogenic potential and regenerative capacity after transplantation, there is large heterogeneity in the cell populations, including non-myogenic cells such as neuronal and mesenchymal cells (Xi et al., 2020), indicating that not all the hiPSC-derived cells are of myogenic lineage. The use of surface markers to purify cells presents an elegant solution to this problem. Because the developmental stage of hiPSC-MuPCs is known to be different from that of adult skeletal muscle tissues (Incitti et al., 2019; Xi et al., 2020; Zhao et al., 2020), previously known surface markers for human SCs may not be suitable for hiPSC-MuPC purification. Therefore, further investigation is required to identify *bona fide* cell-surface markers.

Recently, we reported a new myogenic induction protocol with prolonged Wnt agonist treatment to differentiate hiPSC-MuPCs (Zhao et al., 2020). This protocol showed improved dermomyotome differentiation efficiency compared with other protocols. In our previous study, we generated a *MYF5*-tdTomato reporter iPSC line and found that even the *MYF5*-tdTomato-negative cell population expresses PAX7, a widely accepted marker for quiescent SCs. This finding prompted us to compare the *MYF5*-positive and *PAX7*-positive cell populations to isolate hiPSC-MuPCs.

In the present study, we investigate the transcriptional differences between *PAX7*- and *MYF5*-expressing

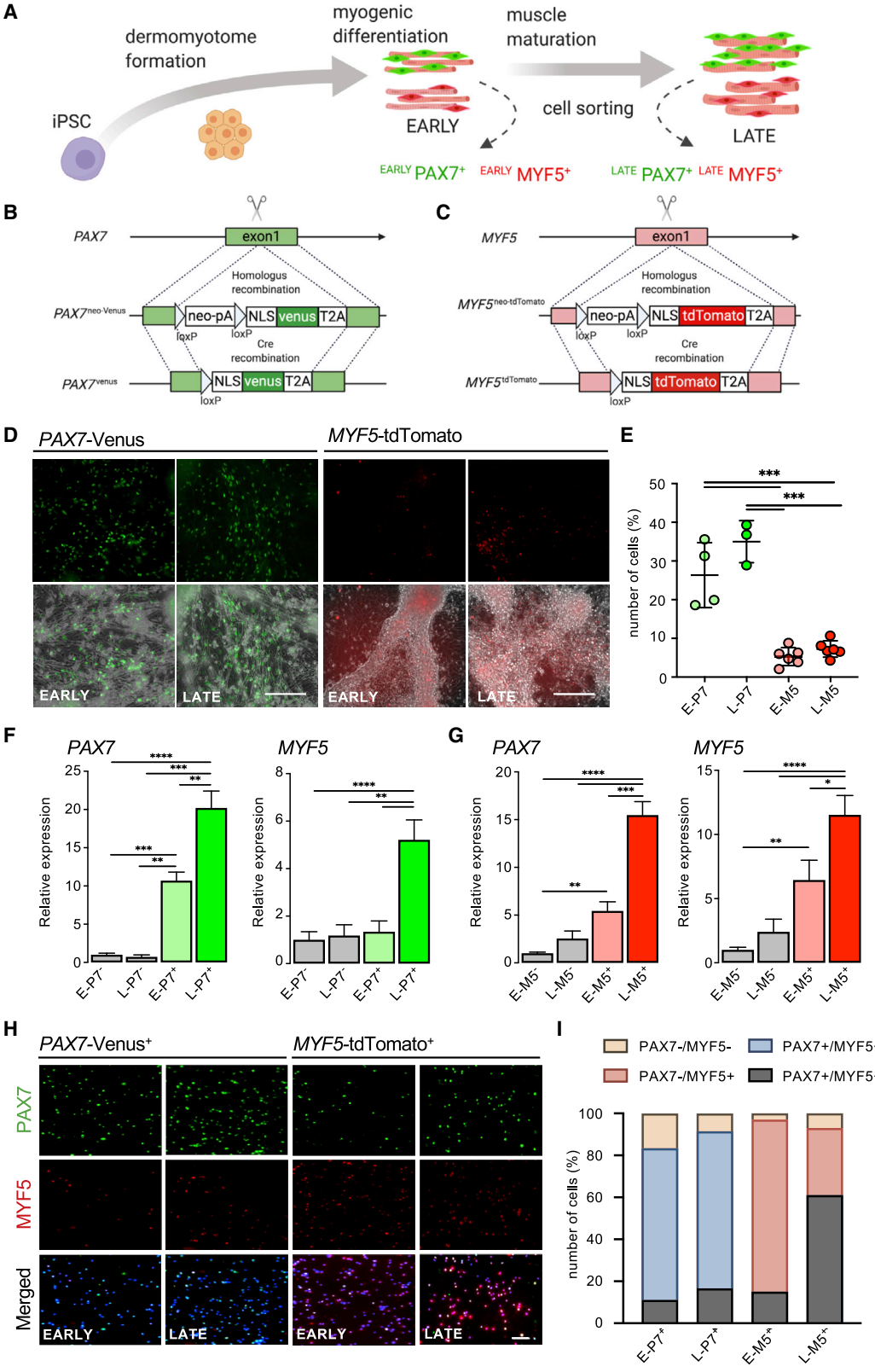

(legend on next page)

hiPSC-MuPC populations. Furthermore, to address the heterogeneity problem, we identified two specific and novel cell-surface markers for the hiPSC-MuPC purification, CDH13 (T-CADHERIN or H-CADHERIN) and FGFR4, which we confirmed are expressed in human fetal skeletal MuPCs. Cell populations positive for either marker showed a high regeneration capacity *in vivo*, including the restoration of dystrophin in Duchenne muscular dystrophy (DMD)-immunodeficient model mice. These markers are expected to benefit studies aiming to generate *in vitro* MuPCs and therapeutic applications.

RESULTS

MYF5-tdTomato and *PAX7*-Venus Reporters Efficiently Identify hiPSC-MuPCs

To generate hiPSC-MuPCs, we used our recently reported stepwise myogenic induction differentiation protocol (Zhao et al., 2020). Because the properties of the hiPSC-MuPCs depend on the culture time, in the present study, we decided to study hiPSC-MuPCs at day 42 (early stage) and day 84 (late stage) of differentiation (Figure 1A).

To identify and purify hiPSC-MuPCs, we established *PAX7*-Venus and *MYF5*-tdTomato reporter cell lines in two different hiPSC lines: 201B7 and S01 (Figures 1B, 1C, and S1A–S1D). After myogenic induction, we observed several twitching colonies (Video S1), in which many Venus-positive and tdTomato-positive cells were located (Videos S2 and S3). We were also able to observe and quantify the tdTomato-positive and Venus-positive cells by flow cytometry (Figure 1D). At the early stage, ~25% of mononuclear cells were *PAX7*-Venus positive and ~5% were *MYF5*-tdTomato positive, while at the late stage, it was ~35% and ~7% (Figure 1E).

qRT-PCR experiments revealed that *PAX7* and *MYF5* were respectively highly expressed in *PAX7*-Venus-positive and *MYF5*-tdTomato-positive cells compared with their negative counterparts (Figures 1F and 1G), indicating correlation with the reporter systems. Early- and late-stage *MYF5*-tdTomato-positive cells were also enriched for *PAX7*, but only late-stage *PAX7*-Venus-positive cells were enriched for *MYF5*. MYF5 and PAX7 staining (Figure 1H) of freshly sorted cells revealed that most *PAX7*-Venus-positive cells were positive for PAX7 and the majority of *MYF5*-tdTomato-positive cells were positive for MYF5. Furthermore, MYF5 and PAX7 double-positive cells were found in ~65% of *MYF5*-tdTomato-positive late-stage cells, but just ~15% of the other populations (Figure 1I). These data suggest that the majority of late-stage *MYF5*-tdTomato-positive cells were a sub-population of *PAX7*-positive cells.

All cell populations showed robust myogenic differentiation capacity *in vitro* (Figures S1E and S1F). We confirmed that more than 50% of the nuclei located outside of the myotubes were *PAX7*-venus positive (Figures S1G and S1H), suggesting that some of these cells can proliferate as a reserve myogenic cell population (Yoshida et al., 1998) and will not express the major histocompatibility complex (MHC). To study the regeneration capacity, we performed transplantation experiments in NOG-mdx mice (n = 4–6 per group) (Figure S1I). The early-stage cell engraftment capacity was very low compared with late-stage cells (Figures S1J and S1K), indicating that late-stage cells possess higher regeneration capacity. Moreover, the *MYF5*-tdTomato-positive cells showed the highest engraftment capacity.

RNA Sequencing Reveals Maturation-Related Differences between hiPSC-MuPC Populations

To transcriptomically compare different hiPSC-MuPC populations, we performed RNA sequencing (RNA-seq) of sorted early- and late-stage *MYF5*-tdTomato-positive and *PAX7*-Venus-positive cells. Principal component analysis

Figure 1. Myogenic Induction of hiPSCs and Validation of the *PAX7*-Venus and *MYF5*-tdTomato Reporter Cell Lines

(A) Schematic representation of the myogenic induction and the strategy for purifying hiPSC-MuPCs. *PAX7*-Venus-positive and *MYF5*-tdTomato-positive cell lines were sorted at the early (day 42) and late (day 84) stages.

(B) CRISPR-Cas9 knockin strategy to establish the *PAX7*-Venus reporter cell lines.

(C) CRISPR-Cas9 knockin strategy to establish the *MYF5*-tdTomato reporter cell lines.

(D) Representative fluorescence of the reporter cell lines before dissociation. Left: *PAX7*-Venus staining at the early and late stages. Right: images of live early- and late-stage *MYF5*-tdTomato cells in culture. Scale bars, 200 μm.

(E) Quantification by FACS of *PAX7*-Venus-positive and *MYF5*-tdTomato-positive cells at the early and late stages. Error bars represent SEM. ***p < 0.001.

(F and G) Relative mRNA expressions of *PAX7* and *MYF5* in *PAX7*-Venus (F) and *MYF5*-tdTomato (G) positive and negative cells at the early and late stages normalized to *GAPDH*. Data from at least three independent experiments are shown as the mean ± SEM. *p < 0.05, **p < 0.01, ***p < 0.001, and p****<0.0001.

(H and I) Immunohistochemical analysis of *PAX7*-Venus-positive and *MYF5*-tdTomato-positive cells. (H) Freshly sorted cells were seeded for 30 min on laminin 511-coated dishes and fixed with 4% paraformaldehyde. Fixed cells were stained with PAX7 and MYF5 antibodies. Scale bar, 50 μm. (I) $PAX7^+$ and $MYF5^+$ stained cells were quantified. Data shown are from three independent experiments. All data are from the 201B7 cell line. E, early stage; L, late stage.

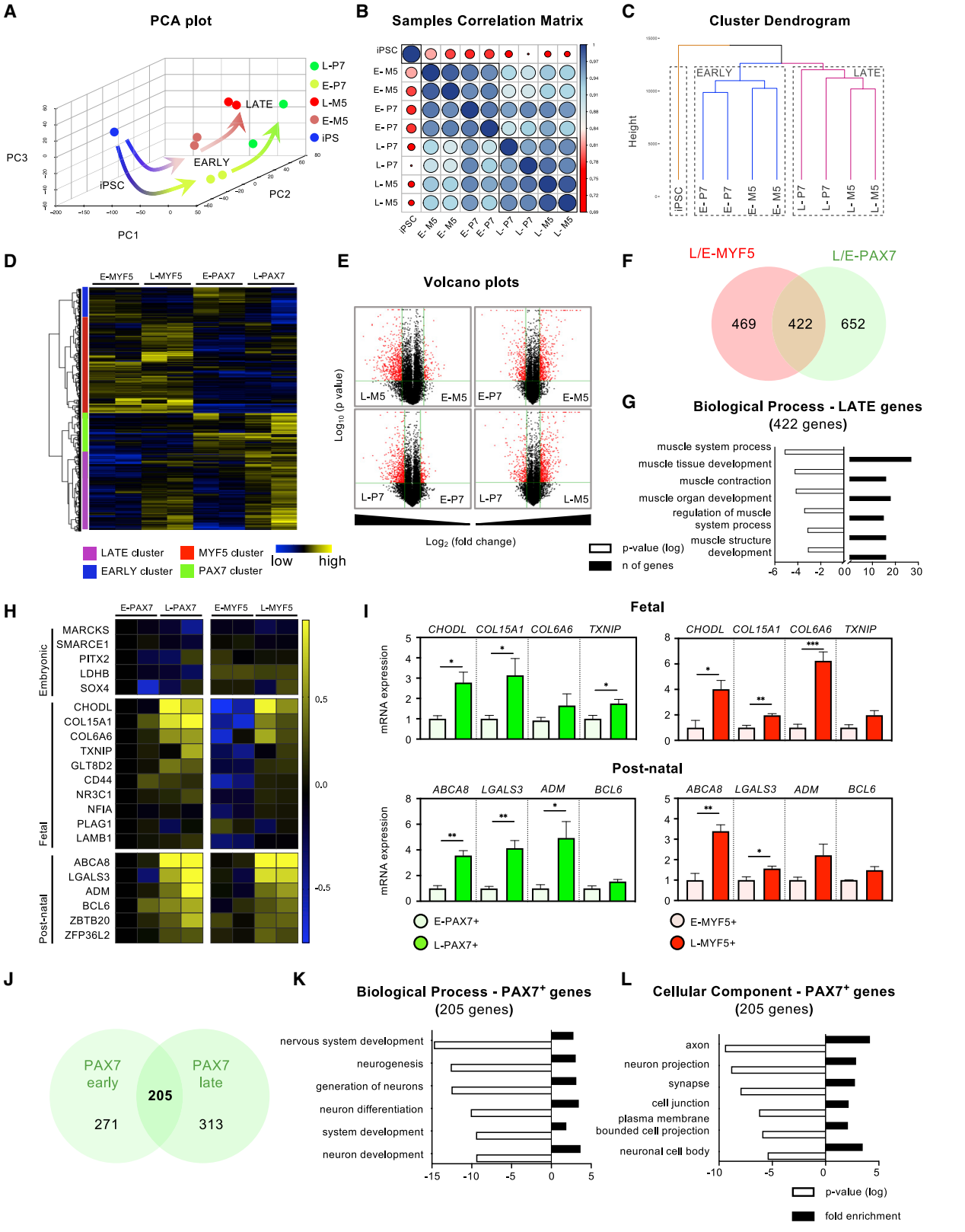

(legend on next page)

revealed that hiPSC-MuPCs are transcriptomically very far from undifferentiated hiPSCs (Figure 2A). Undifferentiated hiPSCs migrated along a trajectory defined by PC1 to early-stage cells, while early-stage cells used a trajectory defined by PC2 to become late-stage cells. In addition, the sample correlation matrix indicated that late-stage cells correlated less with undifferentiated cells than did early-stage cells (Figure 2B). Consistently, a cluster dendrogram revealed that hierarchically late-stage cells grouped separate from early-stage cells (Figure 2C). These results confirmed the culture-time-dependent differences in hiPSC-MuPCs *in vitro*.

As shown in Figures 2D and 2E, we identified hundreds of DEGs (differentially expressed genes: $\geq$2-fold change and $p < 0.05$) between samples. The majority of DEGs between early and late stages consisted of upregulated genes in the late stage (Figure 2D, left), indicating that late-stage cells activated several stage-specific genes. We found that 422 genes were commonly upregulated in late over early stage cells (Figure 2F). GO (gene ontology) analysis revealed that late-stage cells were enriched for biological process terms related to muscle development (Figure 2G), suggesting a time-dependent skeletal muscle lineage specification.

To determine the developmental stage of the different hiPSC-MuPC populations, we plotted the gene signatures of markers related to different developmental stages of human MuPCs (personal communication by Dr. Xi, UCLA) (Figure 2H). Late-stage cells were enriched for fetal and post-natal (juvenile and adult) human markers. We confirmed these results by qRT-PCR (Figure 2I). Extended signatures (Xi et al., 2020) for genes upregulated in MuPCs during development and for the transcriptional program of each developmental stage of human skeletal MuPCs confirmed that late-stage cells were enriched for maturation markers as well as for fetal and post-natal transcription factors (Figures S2A and S2B). These data suggest that late-stage cells possess a more mature phenotype and transcriptomically resemble the fetal/post-natal developmental stage.

To understand the transcriptomic differences between *PAX7*-positive and *MYF5*-positive cells, we studied DEGs between *MYF5*-tdTomato-positive cells and *PAX7*-Venus-positive cells in both stages. Three hundred seventy-four DEGs were upregulated in the two *MYF5*-tdTomato-positive populations (Figure S2C), while 205 DEGs were upregulated in the two *PAX7*-Venus-positive populations (Figure 2J). GO analysis revealed that *MYF5*-tdTomato-positive cells were enriched for terms related to development and cell adhesion (Figure S2D). On the other hand, *PAX7*-Venus-positive cells were enriched for neuron development-related terms (Figures 2K and 2L). We further confirmed gene enrichment for neuron markers in *PAX7*-positive cells (Figures S2E and S2F). These results provide evidence that neuronal-lineage cells expressing *PAX7* are derived from our hiPSC-MuPC differentiation protocol, suggesting that in our culture system, MYF5 possesses a higher efficiency than PAX7 to specify MuPCs.

RNA-Seq Reveals that CDH13 and FGFR4 Surface Markers Enrich Myogenic Capacity and Regenerative Potential *In Vivo*

To uncover new surface markers that could uniquely distinguish myogenic cell populations, we compared the RNA-seq data of *MYF5*-tdTomato-positive and -negative cells (DDBJ: DRA010291) differentiated from hiPSCs (Zhao et al., 2020) (Figure 3A). We identified a total of 993 DEGs ($\geq$2-fold change and $p < 0.05$) between populations, of which 219 were upregulated in *MYF5*-tdTomato-positive and 774 in *MYF5*-tdTomato-negative cells (Figures 3B and 3C). Moreover, GO analysis of the DEGs upregulated in *MYF5*-tdTomato-positive cells indicated that the most distinguished GO term was skeletal muscle satellite cell differentiation (Figure 3D). Furthermore, from the DEGs upregulated in *MYF5*-tdTomato-positive cells, we could identify

Figure 2. Transcriptomic Analysis of hiPSC-MuPCs at Early and Late Stages

(A) Principal component analysis (PCA) plot of *PAX7*-Venus-positive and *MYF5*-tdTomato-positive cells.

(B) Samples correlation matrix. The color scale indicates the Pearson correlation.

(C) Cluster dendrogram of hiPSC-MuPCs (Canberra method).

(D) A heatmap indicating differentially expressed genes (DEGs) between samples (fold change $\geq$2 and $p < 0.05$).

(E) Volcano plots indicating DEGs in red.

(F) A Venn diagram showing DEGs commonly upregulated in late-stage cells.

(G) Gene ontology (GO) terms related to muscle development significantly enriched in late-stage cells.

(H) Heatmap of the skeletal muscle stem cell markers associated with the different developmental stages (relative to early-stage *PAX7*-positive cells).

(I) Relative mRNA expression of representative genes from (E) normalized to *GAPDH*. Data from at least three independent experiments are shown as means ± SEM. *$p < 0.05$, **$p < 0.01$, and ***$p < 0.001$ using Student's t test.

(J) A Venn diagram indicating DEGs upregulated in early- and late-stage *PAX7*-Venus-positive over *MYF5*-tdTomato-positive cells.

(K and L) GO analysis for DEGs. Biological process terms (J) and cellular components terms (K) associated with the upregulated DEGs (H). Data shown in (D and H) are in $\log_{10}$ units. E, early stage; L, late stage.

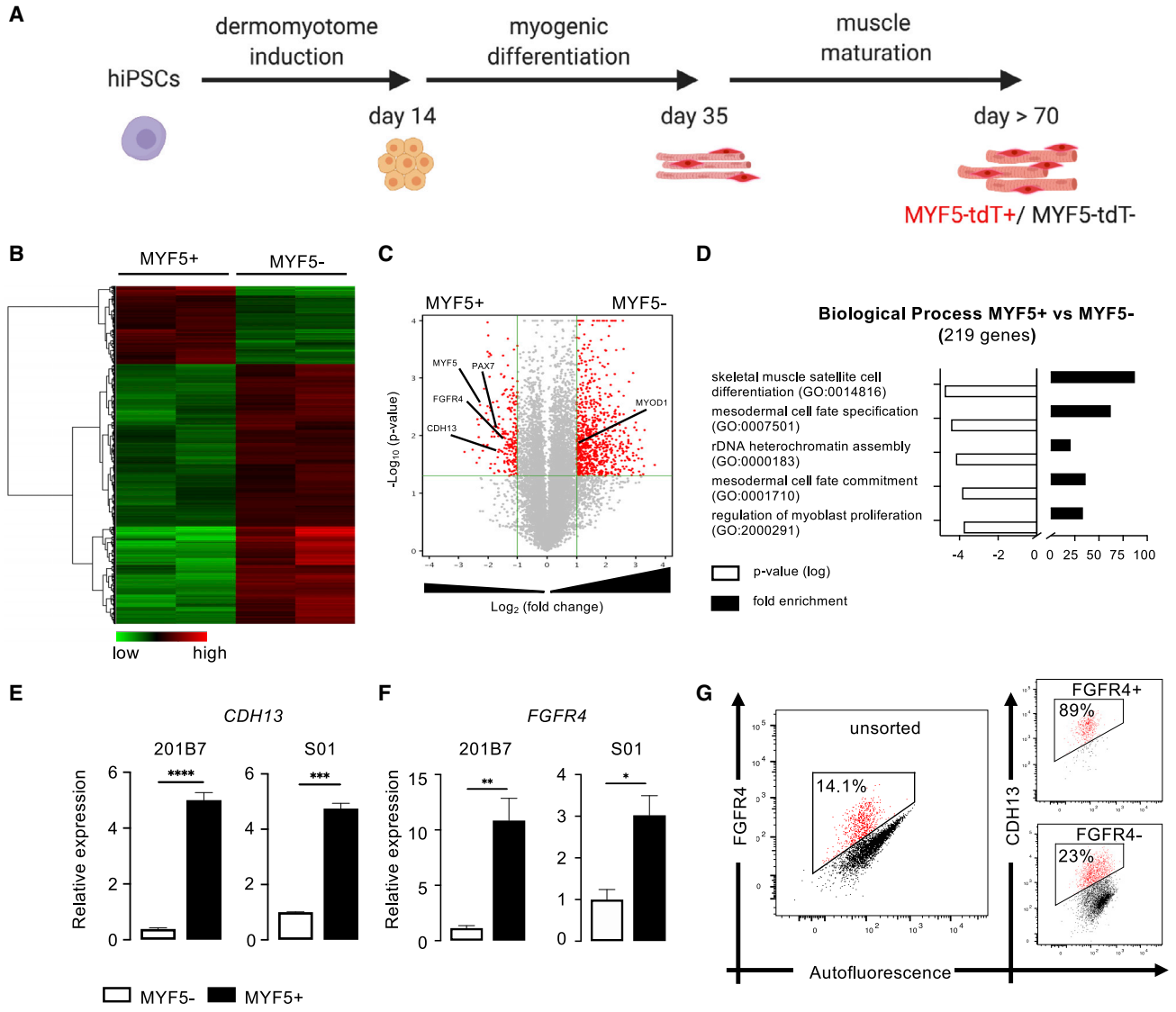

Figure 3. Transcriptomic Analysis of *MYF5*-tdTomato-Positive and -Negative hiPSC-MuPCs

(A) Schematic representation of the myogenic induction and the strategy for purifying hiPSC-MuPCs.

(B and C) Heatmap (B) and volcano plot (C) indicating DEGs (fold change ≥ 2 and $p < 0.05$) between *MYF5*-tdTomato-positive and *MYF5*-tdTomato-negative cells.

(D) GO analysis of DEGs. Biological process terms associated with the *MYF5*-tdTomato-positive over the *MYF5*-tdTomato-negative upregulated DEGs are shown.

(E and F) mRNA expressions of *CDH13* (E) and *FGFR4* (F) in *MYF5*-tdTomato-positive and -negative cells from 201B7 and S01 hiPSCs and quantified by qRT-PCR. Data from at least three independent experiments are shown as means ± SEM. *$p < 0.05$, **$p < 0.01$, ***$p < 0.001$, and ****$p < 0.0001$ using Student's t test.

(G) Representative FACS analysis of late-stage DMD FGFR4-positive DMD-corrected hiPSC-MuPCs for *CDH13* expression.

several cell-surface markers (Table S1). To screen these surface markers, we decided to contrast them with the Human Skeletal Muscle Atlas database (aprilpylelab.com), which is a single-cell RNA-seq database that provides gene expression during human development, as well as with hiPSC-MuPCs differentiated by one of three different protocols: MS (Shelton et al., 2014), JC (Chal et al., 2015) and HX (Xi et al., 2017). We identified *CDH13* and *FGFR4*, which were mostly expressed in skeletal MuPCs across development, with a markedly higher expression during the embryonic and fetal stages (Figures S3A and S3B). To determine whether *CDH13* and *FGFR4* expression was specific

to human MuPCs or common in other animals, we referred to Tabula Muris, a mouse single-cell RNA-seq database (https://tabula-muris.ds.czbiohub.org/; Schaum et al., 2018), which revealed that *Cdh13* and *Fgfr4* are robustly expressed in mouse MuPCs, too (Figures S3C and S3D), but that *Cdh13* is also expressed in endothelial cells (Philippova et al., 2009).

To better understand the expression patterns of these genes in human tissue and whether they are predominantly expressed by skeletal muscle, we used an mRNA-seq database of human tissues surrounding skeletal muscle (GEO: GSE106292). We found that *CDH13* and *FGFR4* were highly expressed in skeletal muscle compared with surrounding tissues (Figures S3E and S3F). After verifying the expression of these markers in skeletal muscle by different databases, we decided to test them for the purification of hiPSC-MuPCs.

First, we confirmed by qRT-PCR *CDH13* and *FGFR4* enrichment in *MYF5*-tdTomato-positive cells (Figures 3E and 3F). Moreover, fluorescence-activated cell sorting (FACS) analysis revealed that ~12% of mononuclear cells were FGFR4 positive and ~23% were CDH13 positive. Moreover, ~90% of FGFR4-positive cells were also CDH13 positive, suggesting that FGFR4-positive cells are a subset of CDH13-positive cells (Figures 3G and S4A). Then we studied the capacity of CDH13 and FGFR4 to enrich the myogenic population of hiPSC-MuPCs. For this purpose, we used three different hiPSC lines: 201B7 (healthy donor), DMD (DMD patient-derived cells), and DMD CRISPR-Cas9-corrected isogenic control (DMD-corrected) (Figure 4A) (Li et al., 2015). CDH13-positive cells were enriched for *MYF5*, *PAX7*, and *MYOD1*, while FGFR4-positive cells were enriched for *MYF5* and *PAX7*, but not *MYOD1* (Figures 4B, 4C, and S4B).

To evaluate the myogenic capacity of CDH13-positive and FGFR4-positive cells, we studied the differentiation capacity *in vitro*. CDH13-positive and FGFR4-positive cells had higher *in vitro* differentiation capacity than their negative counterparts (Figures 4D, 4G, S4C, and S4D). Moreover, we could detect DYSTROPHIN protein in DMD-corrected cells, indicating that this purification method may be useful for *in vitro* disease modeling.

To determine the therapeutic potential of cells purified with CDH13 and FGFR4, we studied their regeneration capacity *in vivo*. Immunohistochemical analysis revealed a superior engraftment capacity in FGFR4-positive and CDH13-positive cells over the negative sorted fractions (n = 3–4 per group). Moreover, FGFR4-positive cells accounted for a higher number of h-SPECTRIN-positive cells (Figures 5A, 5B, and S4E). In addition, in muscle transplanted with cells positive for either of the markers, in the interstitial zone we found hundreds of h-SPECTRIN-positive tiny fibers (i.e., the area of the fiber was not visible as larger than the nuclear area). Because these fibers seem to be *de novo* fibers that had not fused yet with host myofibers, we decided not to include these tiny fibers in the calculation of the engrafted cells (Figures S4F and S4G). Furthermore, DMD-corrected cells restored dystrophin expression in the engrafted fibers (Figure 5C). Interestingly, with either of the markers, we found that some of the transplanted cells were PAX7 positive and positioned beneath the basal lamina and outside of the DYSTROPHIN-positive sarcolemma, which histologically is consistent with SCs (Figures 5D and S4H). Moreover, double staining for PAX7 and MYOD1 indicated that many of the FGFR4-positive transplanted cells express myogenic markers (Figures 5E and 5F). These results suggest that the transplanted cells may also contribute to the muscle stem cell pool and that CDH13 and FGFR4 can be used to efficiently purify myogenic cells with therapeutic potential.

CDH13 and FGFR4 Improve hiPSC-MuPC Purification Compared with Previously Reported Markers

Other surface proteins have been proposed for hiPSC-MuPC purification. To compare CDH13 and FGFR4 with those previously reported markers, we used the Human Skeletal Muscle Atlas to evaluate the single-cell transcriptomics of hiPSC-MuPCs differentiated from the MS, JC, and HX protocols (Figures S5A–S5C). We compared the expression patterns of *FGFR4* and *CDH13* with *NCAM1* (Garcia et al., 2018); *CD82* (Alexander et al., 2016; Uezumi et al., 2016); *NGFR* and *ERBB3* (Hicks et al., 2018); *ICAM1*, *ITGA9*, and *SDC2* (Magli et al., 2017); and *MME* (Wu et al., 2018) across the different protocols. *ICAM1*, *ITGA9*, and *MME* were not expressed by myogenic cells, and *SDS2*, *NCAM1*, and *NGFR* were mostly non-specific for any cell type. On the other hand, *CD82* was robustly expressed by myogenic cells but also marked non-myogenic cells; *ERBB3* was robustly expressed by myogenic cells (mostly by *MYOD1*- and *MYOGENIN*-expressing cells) but enriched as well for other cell types, including Schwann cells; *CDH13* (which was less expressed than the other markers) marked myogenic cells but was expressed as well by other non-myogenic cells; and finally, *FGFR4* was expressed almost exclusively in skeletal MuPCs, especially those expressing *PAX7* and/or *MYF5*. This last finding suggests that as a marker, FGFR4 may give a higher efficiency for purifying hiPSC-MuPCs than the other markers.

Furthermore, the gene expression of these markers was evaluated in *MYF5*-tdTomato-positive and *MYF5*-tdTomato-negative cells. We found that *CDH13*, *FGFR4*, *NGFR*, *ERBB3*, and *CD82* were enriched in *MYF5*-positive cells, while *SDC2*, *NCAM1*, *ITGA9*, *ICAM1*, and *MME* were enriched in *MYF5*-tdTomato-negative cells (Figure S5D).

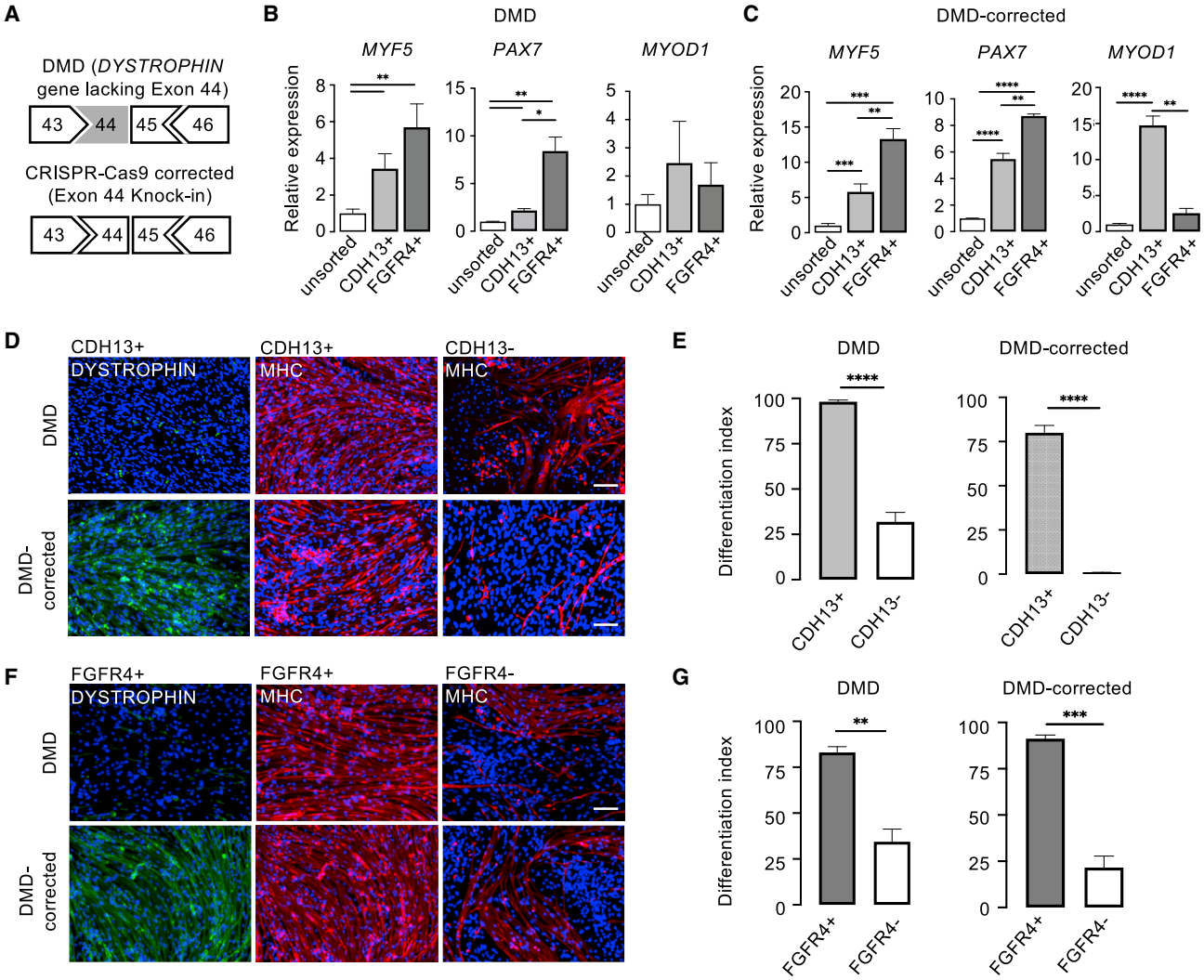

Figure 4. Evaluation of Myogenic Capacity of CDH13-Positive and FGFR4-Positive Cells

(A) A scheme of the DMD-patient-derived hiPSC line and CRISPR-Cas9 knockin DMD-corrected isogenic control cell line.

(B and C) Relative mRNA expression of *PAX7*, *MYF5*, and *MYOD1* normalized to *GAPDH* in CDH13-positive and FGFR4-positive cells relative to unsorted cells in DMD (B) and DMD-corrected (C) hiPSC lines.

(D–G) *In vitro* differentiation of freshly sorted CDH13-positive and -negative cells and FGFR4-positive and -negative cells. Representative immunofluorescence of MHC (red), DYSTROPHIN (green), and DAPI (blue) in CDH13-positive and -negative cells (D) and in FGFR4-positive and -negative cells (F). Scale bars, 200 μm. The differentiation index (% of DAPI positive in the MHC area) was calculated for the DMD (E) and DMD-corrected (G) cell lines.

Data shown in (B and C) and (E and G) are from at least three independent experiments and shown as means ± SEM. *p < 0.05, **p < 0.01, ***p < 0.001, and ****p < 0.0001.

To extrapolate these results to our hiPSC myogenic induction protocol, we tested the markers that were enriched in *MYF5*-tdTomato-positive cells for hiPSC-MuPC purification in our DMD and DMD-corrected cell lines. We found that, consistent with the single-cell RNA-seq data, NCAM1 and NGFR marked over 50% of the cells, while CD82, ERBB3, CDH13, and FGFR4 marked between 15% and 30% (Figures 6A and 6B, left). To characterize the sorted cells, we first studied the gene expression of *MYF5*, *PAX7*, and *MYOD1*. We found that all the markers enriched these three genes. Importantly, CDH13-positive cells and FGFR4-positive cells were the most enriched for *MYF5* and *PAX7* (Figures 6A and 6B). On the other hand, again consistent with single-cell RNA-seq data, FGFR4-positive cells were less enriched for *MYOD1*.

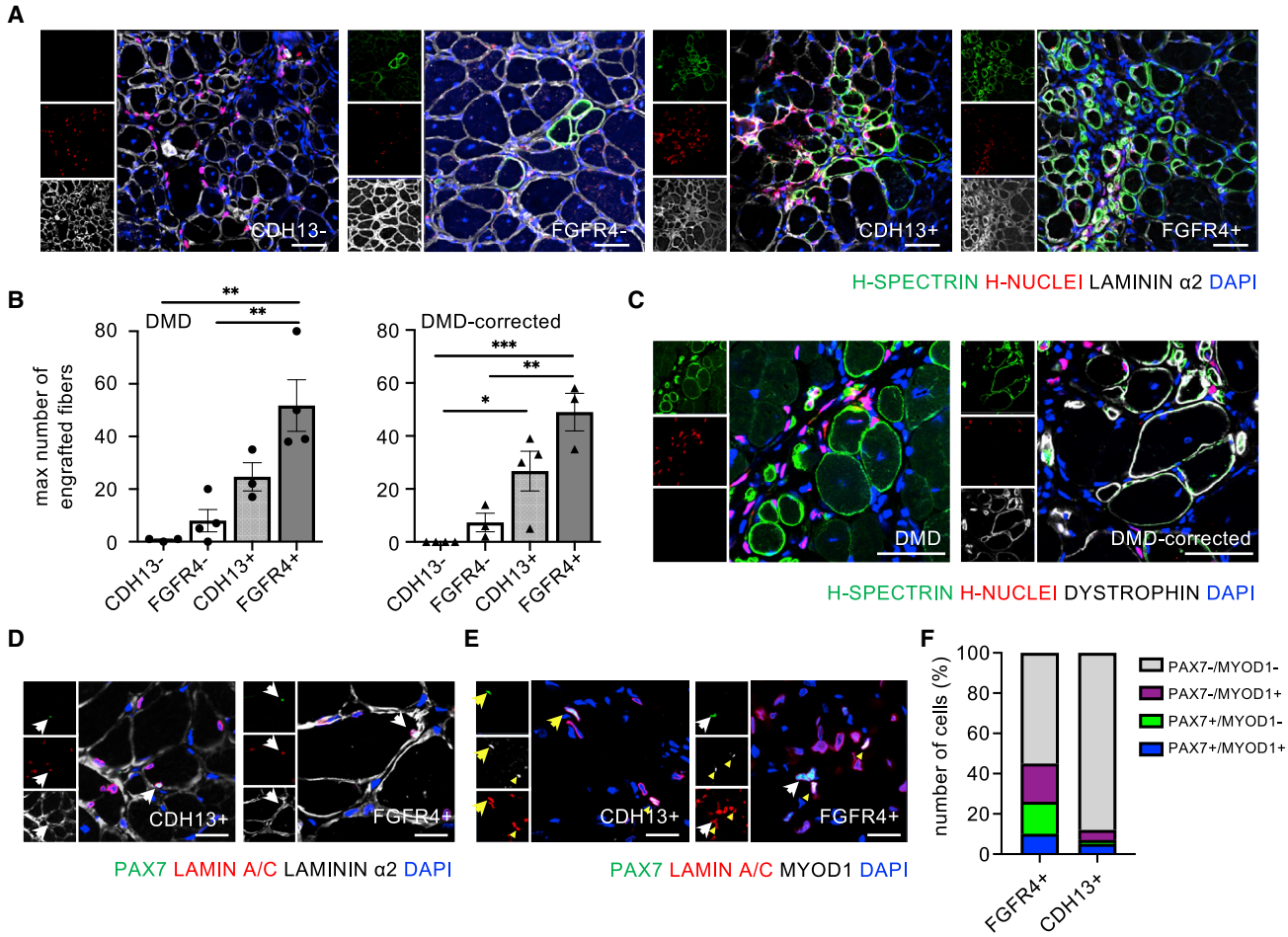

Figure 5. Evaluation of the Regenerative Capacity of CDH13-Positive and FGFR4-Positive Cells in *mdx* Mice

CDH13-positive and -negative cells (1×10^5) and FGFR4-positive and -negative cells (1×10^5) were transplanted into cryo-injured tibialis anterior (TA) muscle in NOG-mdx mice (n = 3 or 4 per group). The regeneration capacity was evaluated 4 weeks after the transplantation by the number of engrafted myofibers.

(A) Representative immunofluorescence of h-NUCLEI (red), h-SPECRIN (green), LAMININ α2 (white), and DAPI (blue) in the transplanted mice. Scale bars, 50 μm.

(B) The maximum number of h-SPECTRIN-positive myofibers per cross-sectional area. Dots represent DMD data (left) and triangles represent DMD-corrected data (right). Data are shown as means ± SEM. *p < 0.05, **p < 0.01, and ***p < 0.001.

(C) Immunofluorescence of DYSTROPHIN (white), h-NUCLEI (red), h-SPECTRIN (green), and DAPI (blue) indicates DYSTROPHIN restoration in engrafted fibers with DMD-corrected-derived cells. Scale bars, 50 μm.

(D) Immunofluorescence of LAMININ α2 (white), PAX7 (green), LAMIN A/C (red), and DAPI (blue) indicates that some human PAX7-positive cells were located inside the basement membrane (LAMININ α2). White arrowheads indicate PAX7-positive cells. Scale bars, 20 μm.

(E) Immunofluorescence of LAMIN A/C (red), PAX7 (green), MYOD1 (white), and DAPI (blue) indicates that 4 weeks after the transplantation, some human cells are PAX7 and/or MOD1 positive. Scale bars, 20 μm. White arrowheads indicate human PAX7-positive/MYOD1-negative cells; yellow arrowheads indicate PAX7-positive/MYOD1-positive cells; and yellow triangles indicate PAX7-negative/MYOD1-positive cells.

(F) Quantification of (E).

To compare the myogenic capacity between sorted cell populations, we performed *in vitro* differentiation (Figures S6A and S6B). All sorted cell populations could give rise to myotubes, but CDH13-positive and FGFR4-positive cells showed the highest differentiation capacity. By using a *PAX7*-Venus hiPSC reporter line, we also analyzed the percentage of *PAX7*-positive cells among the different sorted populations (Figures 6C and 6D). FACS analysis revealed

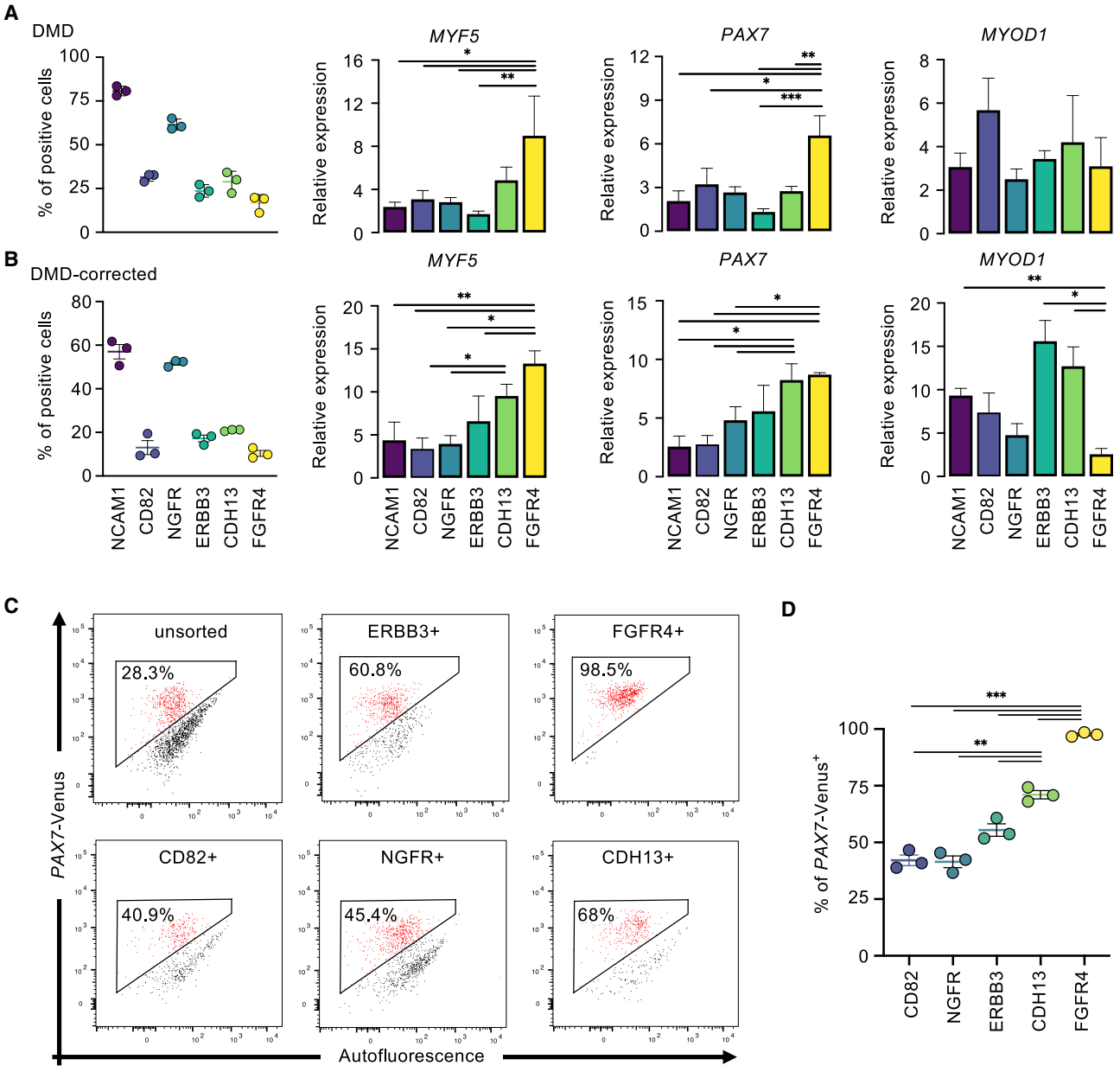

Figure 6. Comparative Analysis of Different Surface Markers for hiPSC-MuPC Purification

(A and B) DMD (A) and DMD-corrected (B) hiPSC-MuPCs were sorted by using different surface protein antibodies. The percentage of positive cells was quantified by FACS analysis (left plot). Freshly sorted cells were analyzed for the gene expression of *MYF5*, *PAX7*, and *MYOD1* by qRT-PCR.

(C) Representative FACS data of hiPSC-MuPCs derived from *PAX7*-Venus 201B7 hiPS differentiated cells and purified with different antibodies.

(D) Quantification of (C).

Data shown in (A), (B), and (D) are from at least three independent experiments and shown as means ± SEM. *$p < 0.05$, **$p < 0.01$, and ***$p < 0.001$.

that CD82 and NGFR enriched for ~40% of *PAX7*-Venus-positive cells, ERBB3 for ~60%, CDH13 for ~70%, and FGFR4 for ~95%.

To study possible contamination by non-myogenic cell lineages, we examined the gene expression of neuronal progenitor cell markers. Because the Human Skeletal

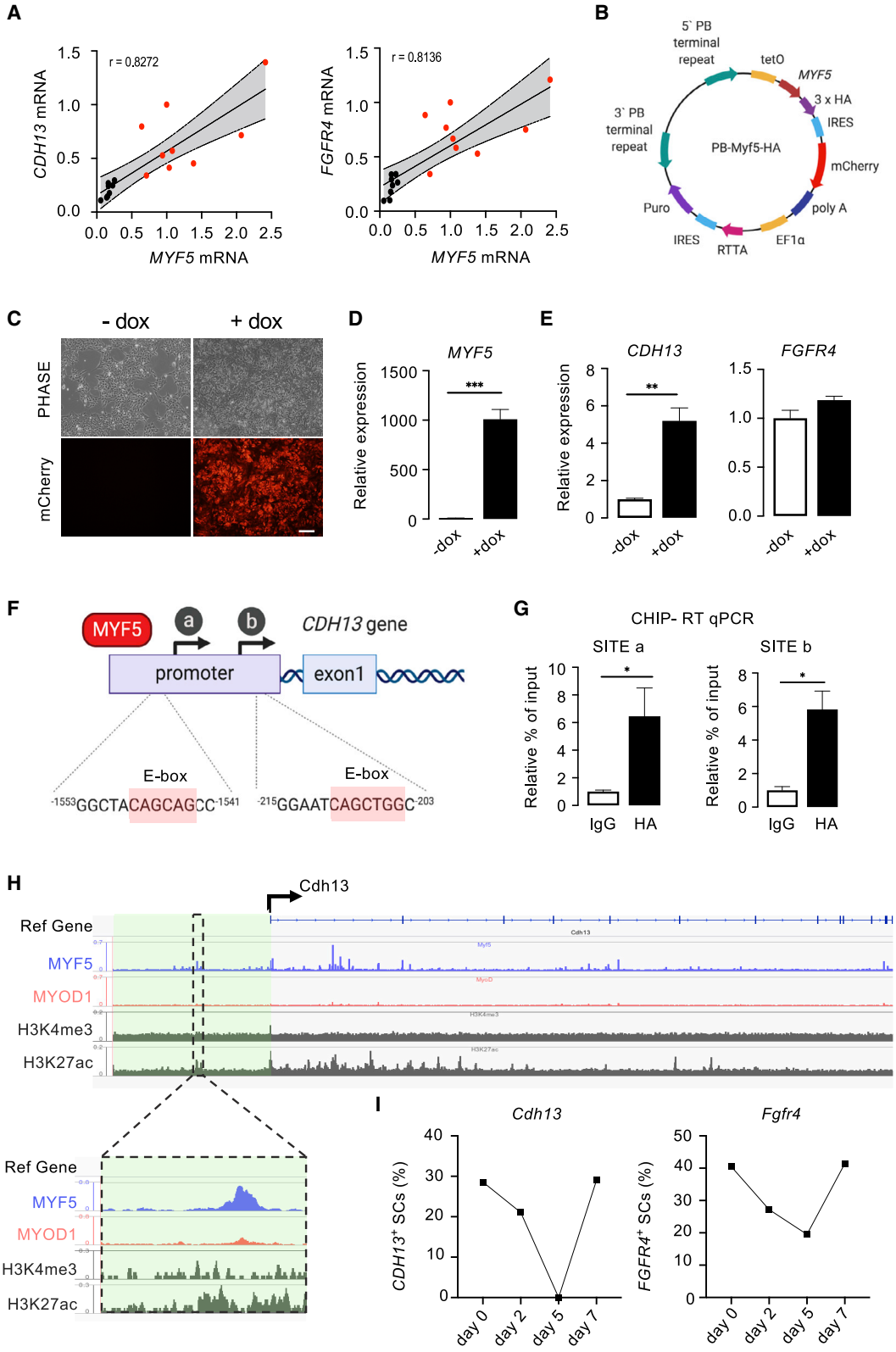

(legend on next page)

Muscle Atlas indicated Schwann cells could contaminate our protocol, we analyzed the expression of markers for Schwann cell progenitors (Kim et al., 2017) (Figure S6C). We found that ERBB3 and, to a lesser extent, NCAM1 and NGFR were expressed with Schwann cell progenitor markers, but CD82, CDH13, and FGFR4 were less so. These results suggest that CDH13 and FGFR4 markers purify myogenic cells at higher efficiency than previously reported markers.

CDH13 Transcription Is Directly Regulated by MYF5

Because *CDH13* and *FGFR4* were found to be enriched in *MYF5*-tdTomato-positive hiPSC-MuPCs, we hypothesized that MYF5 might control the expression of these genes. Indeed, we found a strong correlation between *MYF5* and *CDH13* expression and between *MYF5* and *FGFR4* expression in hiPSC-MuPCs (Figure 7A). To elucidate the possible regulatory mechanism of MYF5 on *CDH13* and *FGFR4* expression, we investigated whether *MYF5* overexpression may induce *CDH13* and/or *FGFR4* expression. We transfected hiPSCs (201B7) with a doxycycline-inducible mCherry-HA-*MYF5* expression vector (Figure 7B) and observed that most of the cells were mCherry positive, indicating the efficacy of the transfection (Figure 7C). Moreover, we confirmed by qRT-PCR that *MYF5* was efficiently overexpressed in doxycycline-treated cells (Figure 7D). Further, *CDH13* expression was increased in *MYF5*-overexpressing undifferentiated hiPSCs, but *FGFR4* expression was unchanged (Figure 7E), suggesting that *CDH13* gene expression, but not *FGFR4*, is regulated by MYF5. Previously, *Fgfr4* has been shown to be downstream of PAX3 in mouse embryo myogenic progenitor cells (Lagha et al., 2008) and in hiPSC-MuPCs (Magli et al., 2019), which could explain why *FGFR4* is expressed in hiPS-MuPCs.

To verify the MYF5 control over *CDH13* expression, we analyzed possible MYF5 binding motifs in the promoter region of *CDH13*. We found putative binding sites in the *CDH13* promoter region, with both sequences containing the E-box binding motif (Figure 7F) (Tierney et al., 2016). To confirm if MYF5 bound to these sites, we performed chromatin immunoprecipitation (ChIP) for MYF5 followed by qRT-PCR. qRT-PCR analysis revealed that DNA fragments precipitated by the hemagglutinin (HA) antibody were enriched for the predicted binding site sequences (Figure 7G), confirming that MYF5 promotes *CDH13* expression by directly binding to the CDH13 promoter region at two different E-box sequences.

Previously, MYF5 and MYOD1 ChIP-sequencing experiments were reported for mouse SCs (GEO: GSE75370) (Conerly et al., 2016). By using the available database, we found that the MYF5-binding signal was strong in the promoter region of *Cdh13*, suggesting that the regulation of *Cdh13* by MYF5 is conserved between mice and humans (Figure 7H). In addition, we analyzed previously published ChIP-sequencing data for chromatin histone modifications in mouse quiescent SCs (GEO: GSE103163) (Machado et al., 2017). We found an increased signal in H3K27ac and H3K4me3 next to the MYF5-binding binding signal, suggesting again a regulatory site for MYF5 (Figure 7H, bottom). We contrasted these results with other single-cell RNA-seq data of activated and quiescent mouse SCs (De Micheli et al., 2020a). In that study, single-cell RNA-seq was performed before the injury and at 2, 5, and 7 days after the injury. By analyzing the available data (GEO: GSE143437), we found that when activated (i.e., after injury), the number of *Cdh13*-positive and *Fgfr4*-positive SCs was decreased. Moreover, 7 days after the injury, the gene expression returned to the level before the injury (Figure 7I). These data suggest that quiescent SCs in mouse express *Cdh13* and *Fgfr4*, which is consistent with our results for hiPSC-MuPCs, where CDH13-positive and FGFR4-positive cells were enriched for *PAX7* and *MYF5*

Figure 7. MYF5 Regulates *CDH13* Gene Expression

(A) Plots showing correlations between *CDH13* and *MYF5* relative expression (left) and between *FGFR4* and *MYF5* relative expression (right). Cells used were *MYF5*-tdTomato(201B7) positive (red dots) or negative (black dots). The gray areas represent 95% confidence bounds.

(B) The PB-MYF5-HA vector construct.

(C and D) *MYF5* overexpression in hiPSCs (201B7). (C) Representative bright-field (PHASE) and mCherry images of live cultures of hiPSCs transfected with the PB-MYF5-HA vector and treated for 3 days with doxycycline (+dox) or a negative control without doxycycline (−dox). Scale bar, 200 μm. (D) Relative mRNA expression of *MYF5* in transfected cells.

(E) Relative mRNA expression of *CDH13* and *FGFR4* in *MYF5*-overexpressing cells.

(F) Representative scheme of the predicted MYF5 binding sites in the *CDH13* gene promoter region.

(G) ChIP-RT-qPCR was performed for HA antibody on the predicted MYF5 binding sites in the *CDH13* promoter region. The percentage of input was normalized to an IgG control.

(H) Integrative Genomics Viewer snapshot displaying the ChIP-seq tracks for MYF5, MYOD1, H3K4me3, and H3K27ac in mouse satellite cells (*Cdh13* region). The black arrow represents the transcription start site and green boxes represent the intergenic region.

(I) Analysis of *Cdh13* and *Fgfr4* gene expression based on single-cell RNA-seq for the regeneration process of mouse TA.

Data shown in (A), (D), and (E) represent gene expression normalized to *GAPDH*. Data shown in (D), (E), and (G) are from at least three independent experiments and shown as means ± SEM. *$p < 0.05$, **$p < 0.01$, and ***$p < 0.001$. Gene expression data are normalized to *GAPDH*.

and after transplantation gave rise to PAX7-positive cells located under the basal lamina-like SCs.

DISCUSSION

By using *MYF5* and *PAX7* hiPSC reporter lines, we identified two new markers for myogenic cell purification: CDH13 and FGFR4. Both markers could sort cells that have high *in vivo* regeneration capacity and *in vitro* differentiation potential. In addition, we showed that *CDH13* expression is regulated by MYF5.

MYF5 is known to be the first of the four myogenic regulatory factors (*MYF5*, *MYOD1*, *MYOGENIN,* and *MRF4*) expressed during mammalian skeletal muscle development (Ott et al., 1991). Notably, one study suggested that *MYF5*-positive fetal MuPCs are the primary source of adult SCs, but *MYF5*-positive embryonic MuPCs made a much smaller contribution (Biressi et al., 2013). This finding is consistent with late-stage *MYF5*-tdTomato-positive cells having higher regenerative and therapeutic potential. On the other hand, *PAX7*, which has been suggested to promote the progression of somatic progenitors into the myogenic lineage and is recognized as a marker of SCs (Seale et al., 2000), is also a non-skeletal muscle-specific gene and known to be expressed in the developing central nervous system and neural crest lineage cells (Buckingham and Relaix, 2007). Consistently, we found that *PAX7*-Venus-positive cells were also enriched for genes related to neuron development, suggesting that in our culture system, *PAX7*-Venus-positive cells might include neuronal lineage cells. Similarly, single-cell RNA-seq analysis of *PAX7*-positive cells prepared from different myogenic induction protocols indicated the contamination of neuronal lineage cells in the sorted cell populations (Xi et al., 2020).

Cell heterogeneity and non-myogenic lineage have been described in several myogenic induction protocols (Xi et al., 2020). Moreover, the transplantation of unsorted hiPSC-MuPCs resulted in extremely poor regeneration capacity (Hicks et al., 2018). Previously reported markers for adult SCs, like NCAM1 and CD82 (Figures 6 and S5) or ITGA7, MCAM, C-MET, CXCR4, and CD11b (Hicks et al., 2018), have been shown to be unsuitable for purifying myogenic cells, probably because the developmental stage of hiPSC-MuPCs is rather fetal and different from that of adult skeletal muscle tissues (Incitti et al., 2019; Xi et al., 2020; Zhao et al., 2020).

We are not the only group to have reported surface markers specific for hiPSC-MuPCs (Hicks et al., 2018; Magli et al., 2017; Wu et al., 2018). Among them, the most used are ERBB3 and NGFR (Hicks et al., 2018; Kim et al., 2020; Sakai-Takemura et al., 2018), which were identified by analyzing human fetal tissues. We studied these markers in the Human Skeletal Muscle Atlas and found that they are expressed not only by skeletal MuPCs but also by Schwann cells across several myogenic induction methods (Figures S5B and S5C). In our culture system, we confirmed the enriched gene expression of Schwann cell progenitor cell markers on ERBB3-positive and NGFR-positive cells (Figure S6C), suggesting other markers for higher purification are desired.

We identified FGFR4 and CDH13 by characterizing hiPSC-MuPCs. FGFR4 and CDH13 have been consistently shown to be expressed by quiescent SCs in human and mouse based on RNA-seq experiments (De Micheli et al., 2020a, 2020b; Pietrosemoli et al., 2017; Schaum et al., 2018; Xi et al., 2020). Our results showed that the new markers improved the efficacy of hiPSC-MuPC purification, as indicated by the increased expression of *MYF5* and *PAX7* and improved *in vitro* differentiation across different cell lines. Moreover, we confirmed that ~95% of FGFR4-positive cells were *PAX7*-positive cells (Figures 6C and 6D), indicating that FGFR4 can be used to highly purify myogenic precursor cells expressing *PAX7*. Interestingly, the expression of *MYOD1* in FGFR4-positive cells was lowest compared with cells positive for the other tested markers. These findings were supported by our *in vitro* differentiation and transplantation studies, indicating that FGFR4 marks a subset of MuPCs with higher regeneration capacity, while CDH13 marks most myogenic cells.

One of the advantages of using hiPSCs instead of embryonic stem cells is the possibility of transplanting autologous gene-corrected cells (Hallett et al., 2015; Hanna et al., 2007; Shiba et al., 2016). By using CDH13 and FGFR4 as markers, we purified myogenic cells from DMD and DMD-corrected hiPSC-MuPCs. The DMD-corrected cells were able to differentiate *in vitro* into myotubes expressing DYSTROPHIN, and after transplantation they could restore DYSTROPHIN expression in engrafted myotubes, strengthening the suitability of CDH13 and FGFR4 as markers for clinical applications. Moreover, some of the transplanted cells were found to be PAX7 positive and to be localized in the SC position, suggesting a possible contribution to the SC pool. Further studies should address the capacity of these cells to contribute to future rounds of regeneration. Finally, in muscle transplanted with cells expressing either of the markers, we could identify hundreds of h-SPECTRIN-positive tiny fibers, which we speculate are *de novo* fibers that can fuse later to form new fibers, increasing the regeneration potential of the transplanted cells.

In summary, this study identified two new cell-surface markers for the purification of hiPSC-MuPCs: CDH13, which marks the majority of myogenic cells, and FGFR4, which marks a subset of MuPCs with higher regeneration capacity. We believe that these two markers will have

important implications for cell therapy for DMD and for the study of basic muscle development.

EXPERIMENTAL PROCEDURES

Human iPSCs

The hiPSC lines 201B7 (Takahashi et al., 2007), Ff-WJ14s01, DMD, and DMD-corrected were used for all the experiments. Ff-WJ14s01 (an HLA-homozygous iPSC line with the most frequent haplotype in Japan, abbreviated as S01 in this article) was established from cord blood cells by using episomal vectors (Okita et al., 2013) at the Facility for iPS Cell Therapy, CiRA, Kyoto University. S01 was generated under written consent with approval of the Kyoto University Graduate School and Faculty of Medicine Ethics Committee (approval nos. E1762, G567, and Rinsho71). The DMD iPSC line (clone ID: CiRA00111) was prepared from dermal fibroblasts of a DMD patient with a deletion of exon 44 by using episomal vectors (Li et al., 2015). The DMD-corrected iPSC line was generated by knocking in exon 44 into CiRA00111 (Li et al., 2015). CiRA00111 was generated under written consent with approval of the Kyoto University Graduate School and Faculty of Medicine Ethics Committee (approval nos. R0091 and G259).

201B7 and S01 were used to generate the *PAX7*-Venus and *MYF5*-tdTomato reporter lines. All hiPSCs were cultured and maintained under feeder-free culture conditions as previously described (Nakagawa et al., 2014). Briefly, the cells were passaged once a week and cultured on an iMatrix-511 (Nippi) pre-coated dish in StemFit AK02N medium (Ajinomoto).

Statistical Analysis

All statistical analyses were performed using GraphPad Prism version 8.4.1 for Mac OS X (GraphPad Software, San Diego, CA, USA). Differences between two groups were analyzed with two-tailed Student's t test, and differences between three or more groups were analyzed by ANOVA with Tukey's range test for multiple comparisons. Differences were considered significant when the p value was <0.05. For the RNA-seq analysis, genes with at least a 2-fold enrichment and $p < 0.05$ were considered DEGs.

Other Materials and Methods

Other materials and methods can be found in the Supplemental Experimental Procedures section.

Data and Code Availability

The accession number for the RNA-seq reported in this paper is DDBJ: DRA010568.

SUPPLEMENTAL INFORMATION

Supplemental Information can be found online at https://doi.org/10.1016/j.stemcr.2021.03.004.

AUTHOR CONTRIBUTIONS

Conceptualization, H.S., M.N., and M.Z.; Methodology, M.N. and M.Z.; Formal Analysis, M.N.; Investigation, M.N., M.Z., M.S.-H., and T.J.; Resources, H.S., A.H., T.M., and M.Y.; Data Curation, M.N.; Discussions, M.N., H.S., M.Z., M.S-H., A.L-C., and Y.Y.; Writing – Original Draft, M.N.; Writing – Review & Editing, M.N., M.Z., and H.S.; Visualization, M.N.; Supervision, H.S. and M.Z.; Funding Acquisition, H.S.

CONFLICT OF INTERESTS

The authors declare that there is a patent being processed in Japan that is related to this work.

ACKNOWLEDGMENTS

We would like to thank Knut Woltjen for sharing some of the plasmids used in this study; April Pyle, Haibin Xi, and Peggie Chien for providing the developmental markers list; Takuya Yamamoto for helping with the data curation; Jun Otomo for valuable scientific discussions; Kanae Mitsunaga for her constant help with the FACS experiments; Masae Sato and Megumi Goto for technical assistance; and Peter Karagiannis for proofreading the manuscript. M.N. especially appreciates his family for continuous support. This work was mainly supported by a grant from The Core Center for iPS Cell Research (19bm0104001h0007) and partially by a grant from The Acceleration Program for Intractable Diseases Research Utilizing Disease-Specific iPS Cells (19bm0804005h0003), both of which are programs in the Research Center Network for Realization of Regenerative Medicine provided by the Japan Agency for Medical Research and Development, AMED (to H.S.).

Received: December 8, 2020
Revised: March 2, 2021
Accepted: March 2, 2021
Published: April 1, 2021

REFERENCES

Alexander, M.S., Rozkalne, A., Colletta, A., Spinazzola, J.M., Johnson, S., Rahimov, F., Meng, H., Lawlor, M.W., Estrella, E., Kunkel, L.M., et al. (2016). CD82 is a marker for prospective isolation of human muscle satellite cells and is linked to muscular dystrophies. Cell Stem Cell *19*, 800–807.

Biressi, S., Bjornson, C.R., Carlig, P.M., Nishijo, K., Keller, C., and Rando, T.A. (2013). Myf5 expression during fetal myogenesis defines the developmental progenitors of adult satellite cells. Dev. Biol. *379*, 195–207.

Buckingham, M., and Relaix, F. (2007). The role of Pax genes in the development of tissues and organs: Pax3 and Pax7 regulate muscle progenitor cell functions. Annu. Rev. Cell Dev. Biol. *23*, 645–673.

Cerletti, M., Jurga, S., Witczak, C.A., Hirshman, M.F., Shadrach, J.L., Goodyear, L.J., and Wagers, A.J. (2008). Highly efficient, functional engraftment of skeletal muscle stem cells in dystrophic muscles. Cell *134*, 37–47.

Chal, J., Oginuma, M., Al Tanoury, Z., Gobert, B., Sumara, O., Hick, A., Bousson, F., Zidouni, Y., Mursch, C., Moncuquet, P., et al. (2015). Differentiation of pluripotent stem cells to muscle fiber to model Duchenne muscular dystrophy. Nat. Biotechnol. *33*, 962–969.

Conerly, M.L., Yao, Z., Zhong, J.W., Groudine, M., and Tapscott, S.J. (2016). Distinct activities of Myf5 and MyoD indicate separate

roles in skeletal muscle lineage specification and differentiation. Dev. Cell *36*, 375–385.

Darabi, R., Arpke, R.W., Irion, S., Dimos, J.T., Grskovic, M., Kyba, M., and Perlingeiro, R.C. (2012). Human ES- and iPS-derived myogenic progenitors restore DYSTROPHIN and improve contractility upon transplantation in dystrophic mice. Cell Stem Cell *10*, 610–619.

De Micheli, A.J., Laurilliard, E.J., Heinke, C.L., Ravichandran, H., Fraczek, P., Soueid-Baumgarten, S., De Vlaminck, I., Elemento, O., and Cosgrove, B.D. (2020a). Single-cell analysis of the muscle stem cell hierarchy identifies heterotypic communication signals involved in skeletal muscle regeneration. Cell Rep. *30*, 3583–3595.e5.

De Micheli, A.J., Spector, J.A., Elemento, O., and Cosgrove, B.D. (2020b). A reference single-cell transcriptomic atlas of human skeletal muscle tissue reveals bifurcated muscle stem cell populations. Skelet. Muscle *10*, 19.

Garcia, S.M., Tamaki, S., Lee, S., Wong, A., Jose, A., Dreux, J., Kouklis, G., Sbitany, H., Seth, R., Knott, P.D., et al. (2018). High-yield purification, preservation, and serial transplantation of human satellite cells. Stem Cell Reports *10*, 1160–1174.

Gilbert, P.M., Havenstrite, K.L., Magnusson, K.E.G., Sacco, A., Leonardi, N.A., Kraft, P., Nguyen, N.K., Thrun, S., Lutolf, M.P., and Blau, H.M. (2010). Substrate elasticity regulates skeletal muscle stem cell self-renewal in culture. Science *329*, 1078–1081.

Hallett, P.J., Deleidi, M., Astradsson, A., Smith, G.A., Cooper, O., Osborn, T.M., Sundberg, M., Moore, M.A., Perez-Torres, E., Brownell, A.L., et al. (2015). Successful function of autologous iPSC-derived dopamine neurons following transplantation in a non-human primate model of Parkinson's disease. Cell Stem Cell *16*, 269–274.

Hanna, J., Wernig, M., Markoulaki, S., Sun, C.-W., Meissner, A., Cassady, J.P., Beard, C., Brambrink, T., Wu, L.-C., Townes, T.M., et al. (2007). Treatment of sickle cell anemia mouse model with iPS cells generated from autologous skin. Science *318*, 1920–1923.

Hicks, M.R., Hiserodt, J., Paras, K., Fujiwara, W., Eskin, A., Jan, M., Xi, H., Young, C.S., Evseenko, D., Nelson, S.F., et al. (2018). ERBB3 and NGFR mark a distinct skeletal muscle progenitor cell in human development and hPSCs. Nat. Cell Biol. *20*, 46–57.

Incitti, T., Magli, A., Darabi, R., Yuan, C., Lin, K., Arpke, R.W., Azzag, K., Yamamoto, A., Stewart, R., Thomson, J.A., et al. (2019). Pluripotent stem cell-derived myogenic progenitors remodel their molecular signature upon in vivo engraftment. Proc. Natl. Acad. Sci. U S A *116*, 4346–4351.

Kim, E., Wu, F., Wu, X., and Choo, H.J. (2020). Generation of craniofacial myogenic progenitor cells from human induced pluripotent stem cells for skeletal muscle tissue regeneration. Biomaterials *248*, 119995.

Kim, H.S., Lee, J., Lee, D.Y., Kim, Y.D., Kim, J.Y., Lim, H.J., Lim, S., and Cho, Y.S. (2017). Schwann cell precursors from human pluripotent stem cells as a potential therapeutic target for myelin repair. Stem Cell Reports *8*, 1714–1726.

Lagha, M., Kormish, J.D., Rocancourt, D., Manceau, M., Epstein, J.A., Zaret, K.S., Relaix, F., and Buckingham, M.E. (2008). Pax3 regulation of FGF signaling affects the progression of embryonic progenitor cells into the myogenic program. Genes Dev. *22*, 1828–1837.

Li, H.L., Fujimoto, N., Sasakawa, N., Shirai, S., Ohkame, T., Sakuma, T., Tanaka, M., Amano, N., Watanabe, A., Sakurai, H., et al. (2015). Precise correction of the dystrophin gene in duchenne muscular dystrophy patient induced pluripotent stem cells by TALEN and CRISPR-Cas9. Stem Cell Reports *4*, 143–154.

Machado, L., Esteves de Lima, J., Fabre, O., Proux, C., Legendre, R., Szegedi, A., Varet, H., Ingerslev, L.R., Barres, R., Relaix, F., et al. (2017). *In Situ* fixation redefines quiescence and early activation of skeletal muscle stem cells. Cell Rep. *21*, 1982–1993.

Magli, A., Baik, J., Pota, P., Cordero, C.O., Kwak, I.Y., Garry, D.J., Love, P.E., Dynlacht, B.D., and Perlingeiro, R.C.R. (2019). Pax3 cooperates with Ldb1 to direct local chromosome architecture during myogenic lineage specification. Nat. Commun. *10*, 2316.

Magli, A., Incitti, T., Kiley, J., Swanson, S.A., Darabi, R., Rinaldi, F., Selvaraj, S., Yamamoto, A., Tolar, J., Yuan, C., et al. (2017). PAX7 targets, CD54, integrin alpha9beta1, and SDC2, allow isolation of human ESC/iPSC-Derived myogenic progenitors. Cell Rep. *19*, 2867–2877.

Marg, A., Escobar, H., Gloy, S., Kufeld, M., Zacher, J., Spuler, A., Birchmeier, C., Izsvak, Z., and Spuler, S. (2014). Human satellite cells have regenerative capacity and are genetically manipulable. J. Clin. Invest. *124*, 4257–4265.

Mauro, A. (1961). Satellite cell of skeletal muscle fibers. J. Biophysical Biochem. Cytol. *9*, 493–495.

Montarras, D., Morgan, J., Collins, C., Relaix, F., Zaffran, S., Cumano, A., Partridge, T., and Buckingham, M. (2005). Direct isolation of satellite cells for skeletal muscle regeneration. Science *309*, 2064–2067.

Nakagawa, M., Taniguchi, Y., Senda, S., Takizawa, N., Ichisaka, T., Asano, K., Morizane, A., Doi, D., Takahashi, J., Nishizawa, M., et al. (2014). A novel efficient feeder-free culture system for the derivation of human induced pluripotent stem cells. Sci Rep *4*, 3594.

Negroni, E., Riederer, I., Chaouch, S., Belicchi, M., Razini, P., Di Santo, J., Torrente, Y., Butler-Browne, G.S., and Mouly, V. (2009). In vivo myogenic potential of human CD133+ muscle-derived stem cells: a quantitative study. Mol. Ther. *17*, 1771–1778.

Okita, K., Yamakawa, T., Matsumura, Y., Sato, Y., Amano, N., Watanabe, A., Goshima, N., and Yamanaka, Y. (2013). An efficient nonviral method to generate integration-free human-induced pluripotent stem cells from cord blood and peripheral blood cells. Stem Cells *31*, 458–466.

Ott, M.-O., Bober, E., Lyons, G., Arnold, H., and Buckingham, M. (1991). Early expression of the myogenic regulatory gene, myf-5, in precursor cells of skeletal muscle in the mouse embryo. Development *111*, 1097–1107.

Philippova, M., Joshi, M.B., Kyriakakis, E., Pfaff, D., Erne, P., and Resink, T.J. (2009). A guide and guard: the many faces of T-cadherin. Cell Signal. *21*, 1035–1044.

Pietrosemoli, N., Mella, S., Yennek, S., Baghdadi, M.B., Sakai, H., Sambasivan, R., Pala, F., Di Girolamo, D., and Tajbakhsh, S. (2017). Comparison of multiple transcriptomes exposes unified

and divergent features of quiescent and activated skeletal muscle stem cells. Skelet. Muscle *7*, 28.

Relaix, F., and Zammit, P.S. (2012). Satellite cells are essential for skeletal muscle regeneration: the cell on the edge returns centre stage. Development *139*, 2845–2856.

Sacco, A., Doyonnas, R., Kraft, P., Vitorovic, S., and Blau, H.M. (2008). Self-renewal and expansion of single transplanted muscle stem cells. Nature *456*, 502–506.

Sakai-Takemura, F., Narita, A., Masuda, S., Wakamatsu, T., Watanabe, N., Nishiyama, T., Nogami, K., Blanc, M., Takeda, S., and Miyagoe-Suzuki, Y. (2018). Premyogenic progenitors derived from human pluripotent stem cells expand in floating culture and differentiate into transplantable myogenic progenitors. Sci. Rep. *8*, 6555.

Sato, T., Higashioka, K., Sakurai, H., Yamamoto, T., Goshima, N., Ueno, M., and Sotozono, C. (2019). Core transcription factors promote induction of PAX3-positive skeletal muscle stem cells. Stem Cell Reports *13*, 352–365.

Schaum, N., Karkanias, J., Neff, N.F., May, A.P., Quake, S.R., Wyss-Coray, T., and Darmanis, S. (2018). Single-cell transcriptomics of 20 mouse organs creates a Tabula Muris. Nature *562*, 367–372.

Seale, P., Sabourin, L.A., Girgis-Gabardo, A., Mansouri, A., Gruss, P., and Rudnicki, M.A. (2000). Pax7 is required for the specification of myogenic satellite cells. Cell *102*, 777–786.

Shelton, M., Metz, J., Liu, J., Carpenedo, R.L., Demers, S.P., Stanford, W.L., and Skerjanc, I.S. (2014). Derivation and expansion of PAX7-positive muscle progenitors from human and mouse embryonic stem cells. Stem Cell Reports *3*, 516–529.

Shiba, Y., Gomibuchi, T., Seto, T., Wada, Y., Ichimura, H., Tanaka, Y., Ogasawara, T., Okada, K., Shiba, N., Sakamoto, K., et al. (2016). Allogeneic transplantation of iPS cell-derived cardiomyocytes regenerates primate hearts. Nature *538*, 388–391.

Takahashi, K., Tanabe, K., Ohnuki, M., Narita, M., Ichisaka, T., Tomoda, K., and Yamanaka, S. (2007). Induction of pluripotent stem cells from adult human fibroblasts by defined factors. Cell *131*, 861–872.

Tanaka, K.K., Hall, J.K., Troy, A.A., Cornelison, D.D., Majka, S.M., and Olwin, B.B. (2009). Syndecan-4-expressing muscle progenitor cells in the SP engraft as satellite cells during muscle regeneration. Cell Stem Cell *4*, 217–225.

Tierney, M.T., Gromova, A., Sesillo, F.B., Sala, D., Spenle, C., Orend, G., and Sacco, A. (2016). Autonomous extracellular matrix remodeling controls a progressive adaptation in muscle stem cell regenerative capacity during development. Cell Rep. *14*, 1940–1952.

Uezumi, A., Nakatani, M., Ikemoto-Uezumi, M., Yamamoto, N., Morita, M., Yamaguchi, A., Yamada, H., Kasai, T., Masuda, S., Narita, A., et al. (2016). Cell-surface protein profiling identifies distinctive markers of progenitor cells in human skeletal muscle. Stem Cell Reports *7*, 263–278.

Wu, J., Matthias, N., Lo, J., Ortiz-Vitali, J.L., Shieh, A.W., Wang, S.H., and Darabi, R. (2018). A myogenic double-reporter human pluripotent stem cell line allows prospective isolation of skeletal muscle progenitors. Cell Rep. *25*, 1966–1981.e4.

Xi, H., Fujiwara, W., Gonzalez, K., Jan, M., Liebscher, S., Van Handel, B., Schenke-Layland, K., and Pyle, A.D. (2017). In vivo human somitogenesis guides somite development from hPSCs. Cell Rep. *18*, 1573–1585.

Xi, H., Langerman, J., Sabri, S., Chien, P., Young, C.S., Younesi, S., Hicks, M.R., Gonzalez, K., Fujiwara, W., Marzi, J., et al. (2020). A human skeletal muscle atlas identifies the trajectories of stem and progenitor cells across development and from human pluripotent stem cells. Cell Stem Cell *27*, 158–176.e10.

Xu, X., Wilschut, K.J., Kouklis, G., Tian, H., Hesse, R., Garland, C., Sbitany, H., Hansen, S., Seth, R., Knott, P.D., et al. (2015). Human satellite cell transplantation and regeneration from diverse skeletal muscles. Stem Cell Reports *5*, 419–434.

Yoshida, N., Yoshida, S., Koishi, K., Masuda, K., and Nabeshima, Y. (1998). Cell heterogeneity upon myogenic differentiation: down-regulation of MyoD and Myf-5 generates 'reserve cells'. J. Cell Sci. *111*, 769–779.

Zhao, M., Tazumi, A., Takayama, S., Takenaka-Ninagawa, N., Nalbandian, M., Nagai, M., Nakamura, Y., Nakasa, M., Watanabe, A., Ikeya, M., et al. (2020). Induced fetal human muscle stem cells with high therapeutic potential in a mouse muscular dystrophy model. Stem Cell Reports *15*, 80–94.